Research article

Application of a neural fuzzy model combined with simulated annealing algorithm to predict optimal conditions for polyethylene waste non-isothermal pyrolysis

Ruming Pan [a], João Vitor Ferreira Duque [a,b,c], Márcio Ferreira Martins [c], Gérald Debenest [a,*]

[a] Institut de Mécanique des Fluides de Toulouse (IMFT) - Université de Toulouse, CNRS-INPT-UPS, Toulouse, 31400, France
[b] Federal Institute of Education, Science and Technology of Espírito Santo, Serra, 29173-087, Brazil
[c] Laboratory of Combustion and Combustible Matter (LCC), PPGEM, Federal University of Espírito Santo, Vitória, 29075-910, Brazil

ABSTRACT

In the present study, the waste polyethylene (PE) pyrolysis under different non-isothermal conditions was investigated to estimate the optimal conversions and pyrolysis rates. The pyrolysis study was carried out using Thermogravimetry (TG) of the virgin and the waste PE under different heating rates of 5, 10, 15 and 20 °C/min. The TG experiments indicated that the virgin and the waste PE pyrolysis processes mainly underwent in the temperature range of 390–510 °C. Subsequently, the adaptive neural fuzzy model was adopted to predict the conversions and the pyrolysis rates of the virgin and the waste PE. The optimal operating conditions in different temperature ranges were optimized by the simulated annealing algorithm (SA). Moreover, the R-squared values of the virgin PE conversions (~ 1) and pyrolysis rates (> 0.999), and the waste PE conversions (~ 1) and pyrolysis rates (> 0.999) revealed the high accuracy of the adaptive neural fuzzy model predicted results.

1. Introduction

Due to the growing population, global annual plastic production has reached 129 million tons [1]. However, only a few postconsumer waste plastics were recycled [2]. Consequently, a large amount of plastic waste accumulates in the environment every year [3]. Polyethylene (PE) is the most consumed plastic and the most common type in waste plastics [3]. Waste plastics from municipal solid waste account for around 33 million tons [4]. PE accounted for 29.8 % (12.3 % for high-density PE and 17.5 % for low-density PE) of European plastic converter demand in 2016 [5]. The recycling of waste plastics has become an urgent issue since the discarded plastics have caused hazards to both living creatures and environments [3]. Therefore, it is critical to developing new methods to improve waste PE operation recycling.

Pyrolysis is a promising recycling method that could directly convert the waste PE to fuels. Canopoli et al. [3] conducted the waste PE and polypropylene (PP) pyrolysis investigation. They analyzed the pyrolysis oil characteristics produced from waste PE and PP of different buried time. Dobo et al. [6] investigated the pyrolysis for gasoline productions from the waste PE, PP, polystyrene (PS), polyethylene terephthalate (PET), and polyurethane (PUR). Park et al. [7] investigated the waste PE co-pyrolysis with Quercus variabilis over different types of catalysts. They found that the co-pyrolysis could promote the formation of aromatic compounds. Utami et al. [8] developed an experimental approach that could produce gasoline-range liquid fuel from waste low-density PE. Tomasek et al. [9] also investigated the high-quality liquid fuel production from waste PE. Mangesh et al. [10] explored a pathway to produce diesel engine fuel from different types of waste plastic pyrolysis, e.g. PE and PP. Pyrolyzing PE could also generate gas and solid products. Barbarias et al. [11] utilized high-density PE pyrolysis to produce hydrogen in two series reactors. Esfahani et al. [12] investigated hydrogen-rich syngas and high-quality bio-char production by co-pyrolysis waste high-density PE with coconut shells. Moreover, high-density PE co-cracking with vacuum gasoil could yield dry gas and liquefied petroleum gas, different ranges of liquid fuels and coke [13]. Considering the above background, it is noteworthy that waste PE pyrolysis is a prospective method to relieve environmental pollution and produce different fuels.

According to [14, 15], the temperature and the heating rate are two deterministic parameters in the waste PE pyrolysis process and must be determined to obtaining the optimal conversion and pyrolysis rate. Thus, it is critical to determine the temperature and the heating rate for obtaining the optimal conversion and pyrolysis rate. Teng et al. [16] showed that machine learning, coupled with an optimization algorithm method, is a useful methodology to model thermogravimetric (TG) data and obtain the optimal pyrolysis operating conditions. The same approach could be utilized in the investigation of the waste PE pyrolysis. Dubdub and Al-Yaari [17] adopted an artificial neural network model to determine the low-density PE thermal decomposition kinetic parameters. Herein, the TG experiments at different heating rates are conducted to obtain the original experimental data. Subsequently, the machine learning establishes the mathematical expressions between the heating rate and the temperature, and the waste PE conversion and pyrolysis rate. Lastly, an optimization algorithm is applied to obtain the optimal operating parameters, based on the relevant mathematical expressions.

The adaptive neural fuzzy model is a widely spread machine learning method used to establish a mathematical correlation between the multiple independent and induced variables. Ustun et al. [18] utilized the adaptive neural fuzzy model to determine the effects of proportional and integral coefficients on the induction motor. Betiku et al. [19] investigated the high-acidity palm kernel oil acid pretreating process by the adaptive neural fuzzy model. Consequently, the operating conditions were optimized to obtain the high-efficiency acid pretreatment by adopting an optimization algorithm. Ighose et al. [20] adopted the adaptive neural fuzzy model to optimize the methyl esters production from the Thevetia peruviana seed oil. Khosravi et al. [21] investigated the solar dish performance under different design parameters. The solar dish with superior performance, was sequentially determined by the adaptive neural fuzzy model coupled with an optimization algorithm. Aghbashlo et al. [22] synthesized solketal from glycerol in different operating conditions. They used the adaptive neural fuzzy model to optimize the operating conditions for the maximum solketal production. Furthermore, Sayyaadi et al. applied the adaptive neural fuzzy model to the optimization of the benchmark cogeneration system [23], the energy systems [24] and the steam power plant [25], respectively. Therefore, it is of particular interest to couple the adaptive neural fuzzy model with the optimization algorithm as a promising method to determine the optimal operating conditions with multiple parameters.

This study investigated the waste PE thermal pyrolysis kinetic modeling. The virgin PE thermal pyrolysis was investigated as a reference. The TG experiments at different heating rates were conducted to provide the adaptive neural fuzzy model's training data. The adaptive neural fuzzy model predicted results were compared with the experimental ones to verify its reliability. Furthermore, the simulated annealing algorithm (SA) [26] was adopted to optimize the operating parameters, i.e. the temperature and the heating rate, in different temperature ranges.

2. Materials and methods

This section introduces the materials used in the experiments and the experimental method. Moreover, the adaptive neural fuzzy model and SA are introduced comprehensively in this section.

2.1. PE samples

Two types of low-density PE samples were used in this work. A virgin PE from the petrochemical industry and a waste PE from municipal solid waste, both provided by LukPlast Ind. (ES-Brazil). The samples were used as they were received, i.e., without any further preparation. The virgin PE has a regular geometry with a diameter of around 4 mm and does not have any pigmentation. Since the waste PE is a mixture of plastics, it has irregular geometry with an average particle size of 2 mm and all sort of pigmentations (Figure 1).

2.2. Methods

This sub-section introduces the specific method of the thermogravimetric experiment. The machine learning method, the adaptive neural fuzzy model, and the SA optimization algorithm are described in mathematical expressions.

2.2.1. TG

The thermal decomposition behaviors of the PE samples were obtained from TG experiments. The analysis was carried out on an STA 449F3 from NETZSCH Instruments under an inert atmosphere. A mass sample in the range of 10–15 mg was placed in an Al_2O_3 crucible and progressively heated from 20 to 670 °C at four heating rates, 5, 10, 15, and 20 °C/min. The heating rates were strategically chosen to cover a wide range of pyrolysis processes available in the literature [27, 28, 29, 30, 31]. The conversion (1 – instantaneous mass fraction) and pyrolysis rate (a derivative of conversion against time) could be determined from the experimental data.

2.2.2. Adaptive neural fuzzy model

The heating rate and the temperature were the two independent parameters chosen as governing the virgin and the waste PE pyrolysis processes. Therefore, the conversion and the pyrolysis rate are the dependent values. The adaptive neural fuzzy model can predict these parameters and variables by expressing them as following [18, 19, 21, 24],

$$f(x,y) = \frac{\sum_{i=1}^{n}(a_i \cdot FR_i)}{\sum_{i=1}^{n} FR_i} \tag{1}$$

where x, y, $f(x,y)$, a_i, FR_i and n represent the heating rate, the temperature, the conversion or the pyrolysis rate, the rule constant, the rule value and the number of rules, respectively.
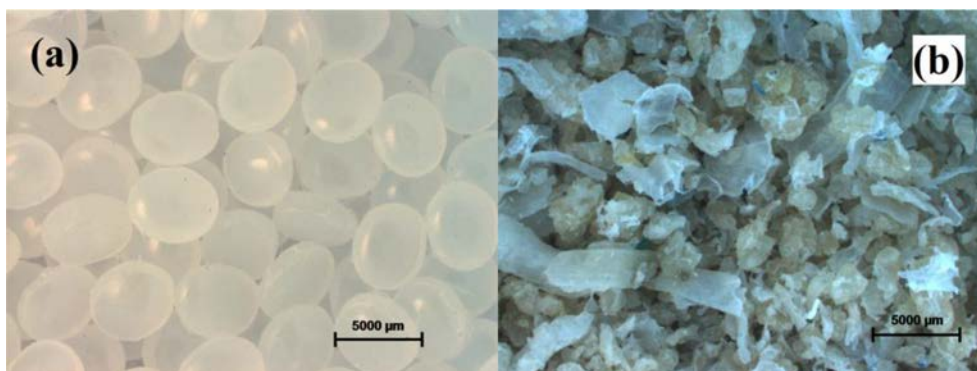

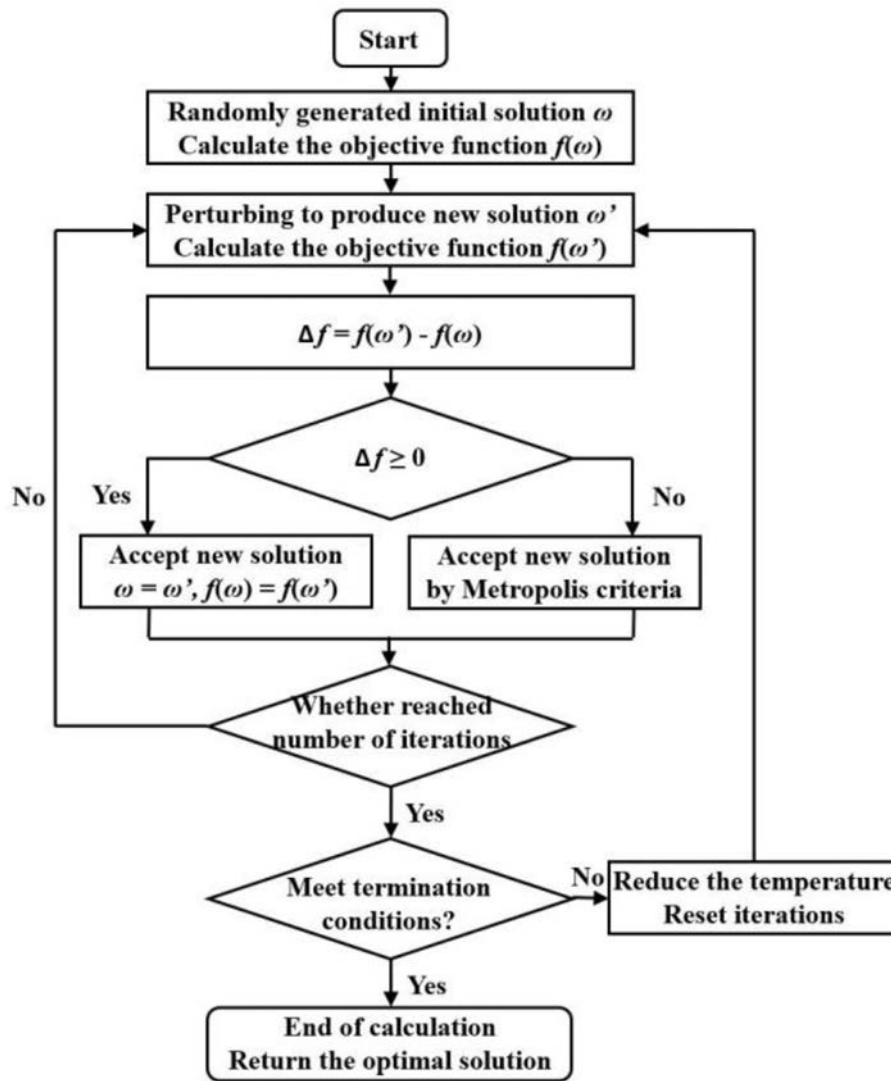**Figure 1.** Low-density PE samples: Virgin PE (a) and Waste PE (b).

Figure 2. SA algorithm flow chart.

The rule value FR_i could be expressed as the following,

$$FR = \begin{bmatrix} u_{x1} \\ \vdots \\ u_{x4} \end{bmatrix} \cdot \begin{bmatrix} u_{y1} & \cdots & u_{y10} \end{bmatrix} \tag{2}$$

where u_{xi} and u_{yj} represent the memberships of the heating rate and the temperature, respectively. The heating rate was divided into 4 levels; and the temperature was divided into 10 levels. Thus, the numbers of the rule constant a_i, the rule value FR_i and the rules n are all 40.

The Gaussian membership function is reported in the literature as a useful tool to obtain the predicted values with higher accuracy [19, 21, 32] and, therefore, was adopted to describe the memberships of the heating rate and the temperature. The memberships of the heating rate and the temperature are expressed as following equations,

$$\mu_{xi} = e^{-0.5 \cdot (x-x_i)^2 / L_{x_i}^2} \tag{3}$$

$$\mu_{yj} = e^{-0.5 \cdot (y-y_j)^2 / L_{y_j}^2} \tag{4}$$

where x_i and y_i, L_{xi} and L_{yi} represent the values of the heating rate and the temperature under different levels, and the Gaussian distribution widths of the heating rate and the temperature, respectively.

2.2.3. SA

SA algorithm illustrated in Figure 2 was utilized to conduct the optimization of the pyrolysis operating conditions. The SA is inspired by the high-temperature liquid metal cooling process [33, 34, 35]. In the cooling process, the metal system's energy decreases and eventually reaches a minimum temperature value [36]. As depicted in Figure 2, in the beginning, the initial solution ω is generated randomly. Furthermore, the objective function $f(\omega)$ is calculated by Eq. (1). The following equations represent the perturbation step,

$$d\omega_{av} = k \cdot T \tag{5}$$

$$d\omega = 0.5 \cdot randn \cdot d\omega_{av} + d\omega_{av} \tag{6}$$

$$\omega' = \omega + d\omega \tag{7}$$

where $d\omega_{av}$, k, T, $d\omega$, $randn$ and ω' are the average displacement distance, the temperature displacement coefficient, the initial temperature, the perturbation, the normally distributed random number and the new solution, respectively.

Subsequently, the new objective function $f(\omega')$ could be calculated. The next step is to calculate the difference Δf between the new objective function $f(\omega')$ and the initial function $f(\omega)$. If Δf is not negative, then the new solution ω' is accepted. Otherwise, the new solution ω' is accepted
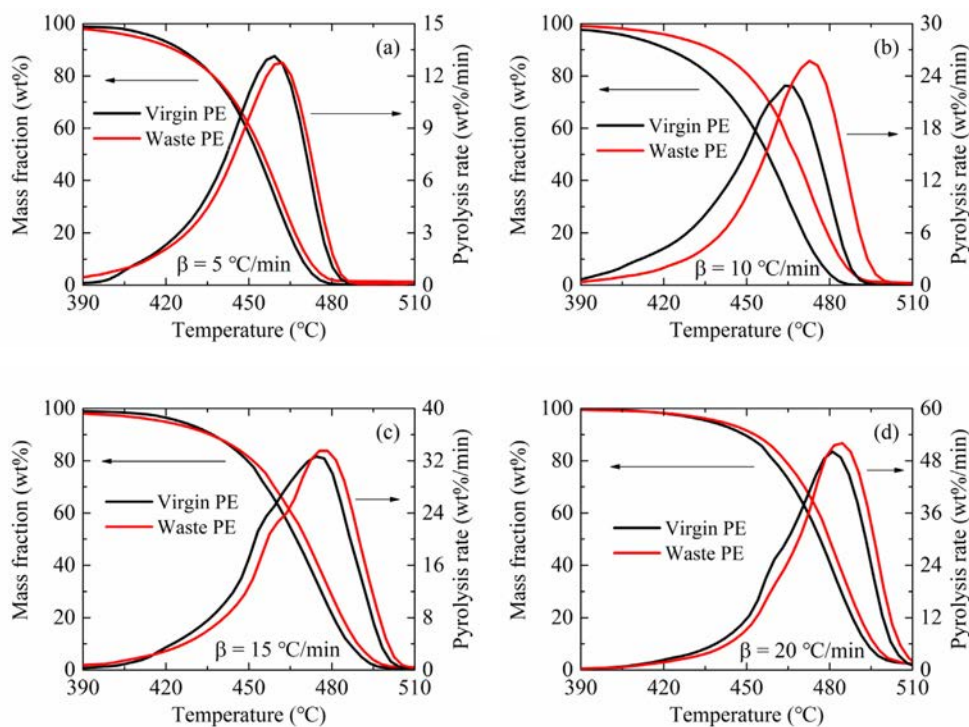
Figure 3. Comparisons of virgin and waste PE mass fractions and pyrolysis rates at different heating rates from 5 °C/min (a), 10 °C/min (b), 15 °C/min (c) to 20 °C/min (d).

by the Metropolis criteria [36, 37]. The following equation expresses the Metropolis criteria,

$$p = \exp(-1 / (k_t \cdot T)) \tag{8}$$

where p and k_t represent the probability of acceptance and the temperature probability coefficient.

After the iteration is complete, the next step is to determine whether it meets the termination conditions. If so, the calculation is finished, and the optimal solution is obtained. Otherwise, it needs to decrease the temperature and repeat the steps mentioned above. The temperature decreasing is expressed by,

$$T' = r_d \cdot T \tag{9}$$

where T' and r_d represent the decreased temperature and the temperature decrease rate.

The initial temperature T, the temperature displacement coefficient k, the temperature probability coefficient k_t, and the temperature decrease rate r_d were investigated in this study to more precisely obtain the optimal operating conditions. Besides, multiple particles could enhance SA optimization performance. Therefore, the number of particles was also investigated.

The adaptive neural fuzzy model and SA were coded and run in MATLAB R2016a with Inter(R) Core (TM) i7-9750H with NVIDIA GeForce GTX 1060.

3. Results and discussion

This section introduces and discusses the virgin and the waste PE TG experimental results firstly. With equal time intervals, one-sixth experimental data was selected to conduct the adaptive neural fuzzy model predictions, another one-sixth experimental data, also with equal time intervals, was selected to evaluate the adaptive neural fuzzy model's accuracy. This data was not covered in the previous predictions. The

virgin PE pyrolysis rate was served as the objective function to determine the SA parameters. Subsequently, SA in different temperature ranges was determined by the virgin and the waste PE optimal conversions and pyrolysis rates.

3.1. TG analysis

Figure 3 illustrates the virgin and the waste PE's mass fractions and pyrolysis rates at the heating rates of 5, 10, 15, and 20 °C/min, respectively. The virgin and the waste PE gradually decomposed as the temperature increased. The mass fraction decreased from 100 to 0 wt% in the temperature range of 390–510 °C. The pyrolysis rate variation could be divided into two stages: increased from 0 wt%/min to the peak value firstly and then decreased to 0 wt%/min in the temperature range of 390–510 °C. Additionally, the mass fraction and pyrolysis rate curves of the virgin and the waste PE shifted laterally to the higher temperatures when the heating rate increased from 5 to 20 °C/min. The reaction mechanism transformations may cause this at different heating rates [38]. For the individual heating rate, the mass fraction and pyrolysis rate curves of the waste PE shifted laterally to the higher temperatures than the virgin one. The same phenomenon was observed in [39], indicating that the waste PE is more challenging to be thermally decomposed than the virgin PE. Moreover, as shown in Figure 3b, the mass fraction and pyrolysis rate curves of the virgin and the waste PE had more significant gaps at 10 °C/min, consistent with the literature [39]. However, to our best knowledge, the abnormality at 10 °C/min has been undetermined to date.

Concerning the conversion rate, the virgin and the waste PE had a single peak at 5, 10, 15, and 20 °C/min. In the literature, the pyrolysis rate curves of the virgin PE [38, 40] and the waste PE [40] also obtained the lone peak at different heating rates. However, it does not suggest that the virgin and the waste PE are decomposed in a one-step mechanism. Both the decompositions of the virgin and the waste PE involve complex multi-step scission reactions. The single peak reveals the overall pyrolysis rate, which practically integrates all the reactions [38].
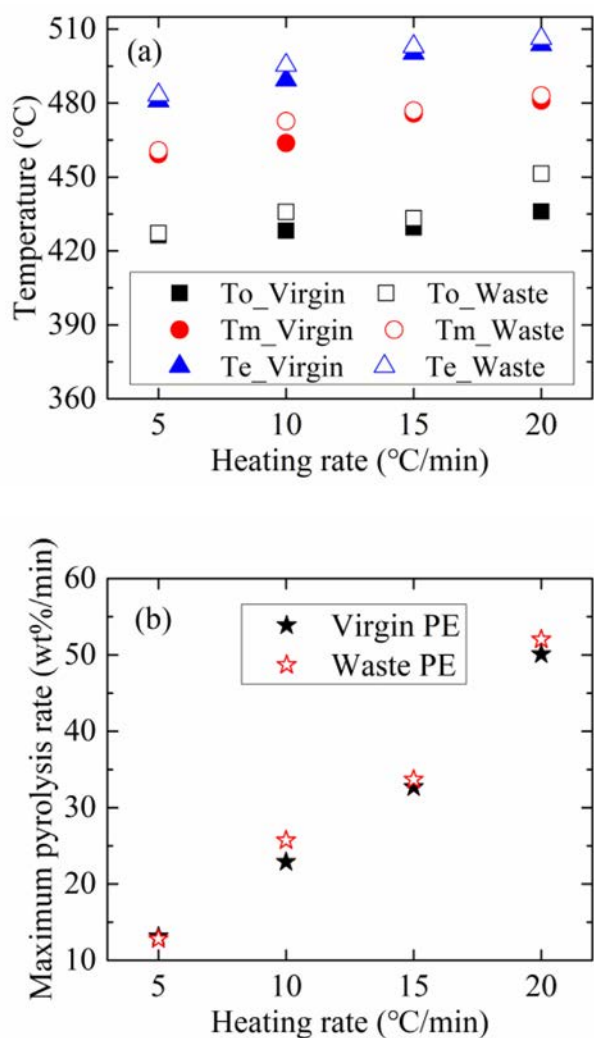
Figure 4. *To, Tm, Te* (a) and maximum pyrolysis rates (b) of the virgin and the waste PE at different heating rates.

The onset temperature (*To*), the temperature at maximum pyrolysis rate (*Tm*), and end temperature (*Te*) were proposed to evaluate the thermal pyrolysis process by different researchers [38, 39, 41]. Figure 4 depicts *To, Tm, Te* and the maximum pyrolysis rates of the virgin and the waste PE at different heating rates. As shown in Figure 4a, the *To, Tm* and *Te* values of the virgin and the waste PE ascended in sequence with the heating rate. The waste PE had higher *To, Tm* and *Te* values than the virgin PE. Besides, the *To, Tm* and *Te* values increased with the heating rate, except for the waste PE's *To* at 10 °C/min. *To* of the waste PE at 10 °C/min was 435.84 °C, while the value was 433.29 °C at 15 °C/min. Figure 4b illustrates the virgin and waste PE's maximum pyrolysis rates at different heating rates. The virgin and the waste PE maximum pyrolysis rates increased from 13.14 to 50.08 wt%/min, and from 12.80 to 52.02 wt%/min when the heating rate increased from 5 to 20 °C/min. Moreover, the waste PE had a higher maximum pyrolysis rate than the virgin PE at the heating rates of 10, 15 and 20 °C/min.

3.2. Mass fraction and pyrolysis rate predicted by the adaptive neural fuzzy model

In the previous subsection, the pyrolysis processes underwent mainly in the temperature range of 390–510 °C at the heating rates of 5, 10, 15, and 20 °C/min. Therefore, the computational calculations by the

adaptive neural fuzzy model were performed inside this range. Besides improving the computation speed, one-sixth part of the experimental data with equal time intervals was selected to conduct the prediction by the adaptive neural fuzzy model.

3.2.1. Virgin PE

Figure 5 demonstrates the mass fraction and the pyrolysis rate of the virgin PE in the temperature range of 390–510 °C, and the heating rate range of 5–20 °C/min. As shown in Figure 5a, the predicted virgin PE's mass fraction had the same variation tendency as the experimental result in Figure 3. The mass fraction decreased from around 100 to 0 wt % when the temperature increased from 390 to 510 °C. The virgin PE's mass fraction surface leaned to the higher temperature and heating rate. It indicated that the virgin PE's decomposition took place in the higher temperature range when the heating rate increased. This corresponds to the experimental results in Figure 3, where the mass fraction curve shifted to a higher temperature at a higher heating rate. Besides, a small bulge emerged near the heating rate of 15 °C/min on the mass fraction surface. The predicted virgin PE's pyrolysis rate surface, as depicted in Figure 5b, is shaped like a ridge. The peak value of virgin PE's pyrolysis rate increased with the heating rate. Moreover, the location of the pyrolysis rate peak at higher heating rates shifted to a higher temperature. It was also consistent with the experimental result, as shown in Figure 3.

3.2.2. Waste PE

Figure 6 depicts the adaptive neural fuzzy model predicted mass fraction and pyrolysis rate of the waste PE, which varied with the
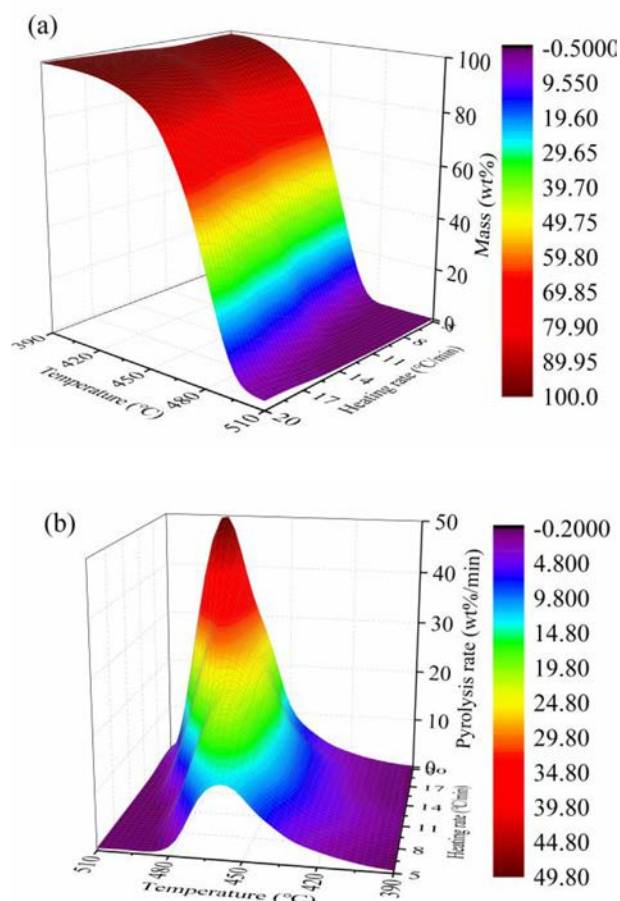

Figure 5. Mass fraction (a) and pyrolysis rate (b) of the virgin PE predicted by the adaptive neural fuzzy model.
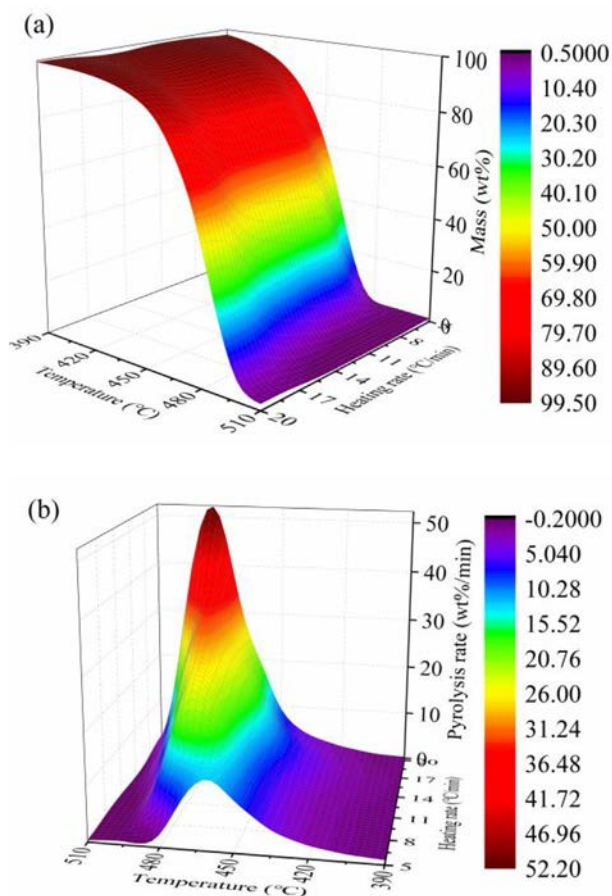
Figure 6. Mass fraction (a) and pyrolysis rate (b) of the waste PE predicted by the adaptive neural fuzzy model.

Figure 7. Mass fraction differences (a) and pyrolysis rate (b) between the waste and the virgin PE predicted results.

temperature and the heating rate. The waste PE mass fraction and the pyrolysis rate surfaces have similar shapes as the virgin PE. However, as shown in Figure 6a, a small bulge emerged near the heating rate of 10 °C/min on the mass fraction surface. The waste PE pyrolysis process was undergoing in the higher temperature range compared to the virgin PE. It coincided with the experimental results in Figure 3, in which the waste PE mass fraction and the conversion rate curves shifted to higher temperatures compared to the virgin PE at different heating rates.

3.2.3. Comparisons of virgin and waste PE

Figure 7 depicts the differences between mass fraction and conversion rate between the waste PE and the virgin PE predicted results. As shown in Figure 7a, the mass fraction difference values were positive in broader heating rates and temperature ranges. The negative mass fraction difference values were in smaller ranges, around 5–7 and 13–20 °C/min, and 390–420 °C. The minimum value was -2.01 wt% at 408 °C and 5 °C/min, while the maximum value was up to 24.28 wt% at 465 °C and 8.75 °C/min. It indicated that the waste PE's thermal pyrolysis process was more difficult to start than the virgin PE [39]. Figure 7b demonstrates the pyrolysis rate differences between the waste and the virgin PE. The virgin PE had a higher pyrolysis rate in a lower temperature range, around 390–480 °C. While in a higher temperature range, around 480–510 °C, the waste PE underwent a faster pyrolysis process. Additionally, the maximum pyrolysis rate difference value was 11.77 wt%/min at the temperature of 480 °C, and the heating rate of 10.62 °C/min. In contrast, the minimum pyrolysis rate difference value was -5.95 wt%/min at the temperature of 465 °C and the heating rate of 20 °C/min.
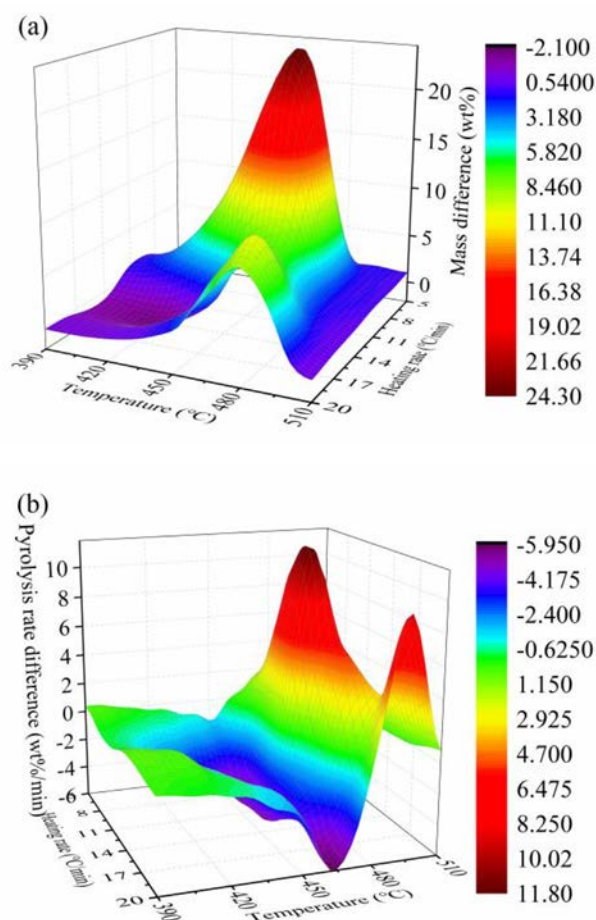
3.3. The accuracy analysis of the adaptive neural fuzzy model

To evaluate the accuracy of the adaptive neural fuzzy model predicted mass fractions and pyrolysis rates, one-sixth part of the experimental data with equal time intervals, which was not covered in the previous predictions, was selected for the verification. Hence, the experimental and predicted results were compared for the virgin and the waste PE. Moreover, the R-squared values were calculated at the heating rates of 5, 10, 15, and 20 °C/min as references.

3.3.1. Virgin PE

Figure 8 shows the experimental and the predicted mass fractions and pyrolysis rates of the virgin PE at the heating rates of 5, 10, 15, and 20 °C/min, respectively. Additionally, the R-squared values between the experimental and predicted results at different heating rates are depicted in Figure 9.

As illustrated in Figure 8, the experimental and predicted mass fraction curves almost coincided with each other. This revealed a high accuracy of the adaptive neural fuzzy model predicted mass fraction. Moreover, as described in Figure 9a, the R-squared values of virgin PE mass fraction were 1, 0.99997, 0.99999, and 0.99999 at the heating rates of 5, 10, 15, and 20 °C/min, respectively.

The adaptive neural fuzzy model predicted mass fraction is much more accurate than the widely used model-free isoconversional method. Aboulkas et al. [42] adopted Friedman's isoconversional method coupled with the "Contracting Sphere" model to investigate the virgin low-density PE thermal degradation behavior. Accordingly, the R-squared value of the virgin low-density PE mass fraction between the experimental and the predicted data was 0.99778 at 10 °C/min. Kim and
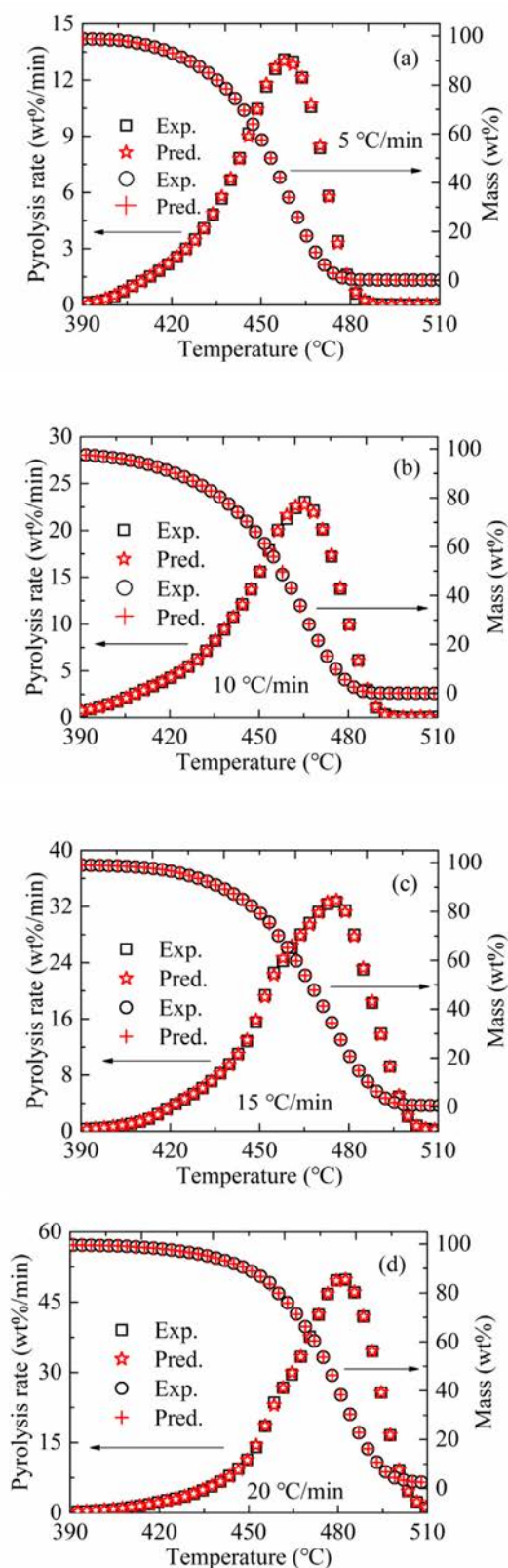
Figure 8. Comparisons of the experimental virgin PE mass fraction and the pyrolysis rate, and the predicted ones by the adaptive neural fuzzy model from 5 °C/min (a), 10 °C/min (b), 15 °C/min (c) to 20 °C/min (d).

Kim [43] adopted isothermal kinetic results coupled with the "Contracting Cylinder" model to investigate high-density PE pyrolysis
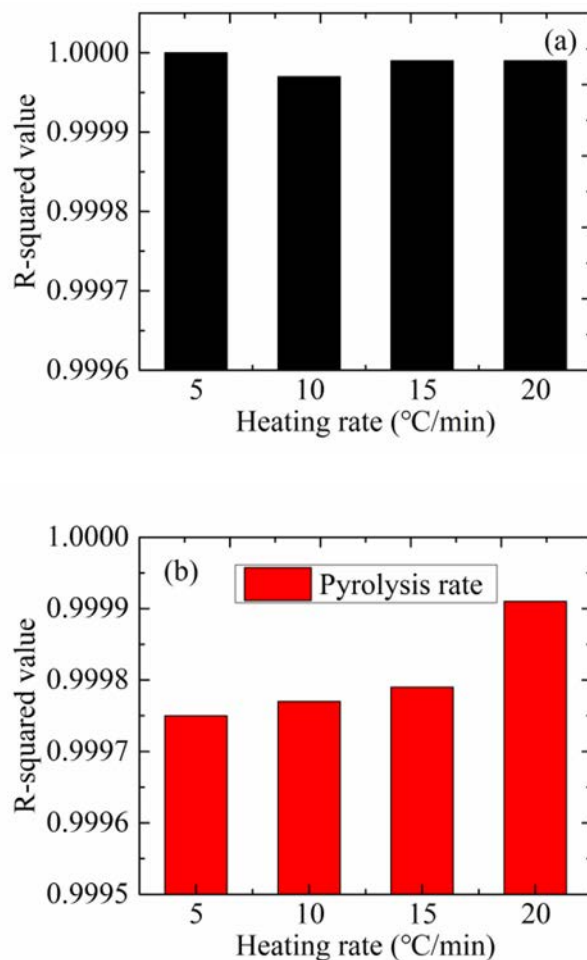

Figure 9. R-squared values of the experimental and the predicted virgin PE mass fractions (a) and pyrolysis rates (b) at different heating rates.

behavior. The average R-squared value of mass fraction was merely 0.984.

The advanced isoconversional method [38] has been reported to be superior to the isoconversional methods. The average R-squared values of low-density PE and high-density PE mass fractions were 0.9990 and 0.9984, respectively. However, the R-squared values are still lower than the results in this study. The fit goodness between the experimental and the predicted results was more unsatisfactory than the mass fraction results for the pyrolysis rate. Nevertheless, the predicted pyrolysis rate could still meet the experimental result to a great extent. As depicted in Figure 8c,d, the predicted pyrolysis rate curves roughened in the temperature range of 450–470 °C, which correspond to the experimental ones. Simultaneously, as demonstrated in Figure 9b, the R-squared values of virgin PE pyrolysis rate were 0.99975, 0.99977, 0.99979, and 0.99991 at the heating rates 5, 10, 15, and 20 °C/min, respectively. The R-squared values were all larger than 0.999. This also exhibited the high accuracy of the adaptive neural fuzzy model predicted the pyrolysis rate.

3.3.2. Waste PE

Figure 10 illustrates the experimental and the predicted mass fractions and pyrolysis rates of the waste PE at the heating rates of 5, 10, 15, and 20 °C/min, respectively. Besides, the R-squared values between the experimental and predicted results at different heating rates are described in Figure 11. As described in Figure 10, the predicted mass fraction fitted the predicted result extraordinary. Figure 11a shows the R-squared values between the experimental and the predicted mass fractions were 1, 0.99998, 0.99998, and 0.99999 at 5, 10, 15, and 20 °C/min,
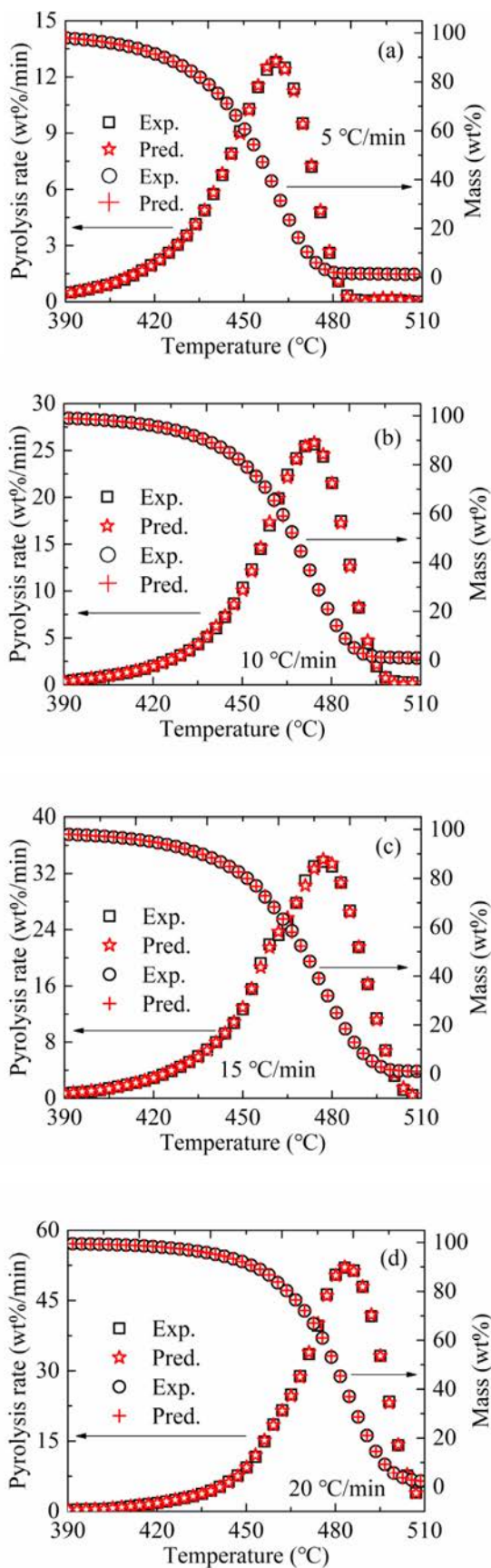
Figure 10. Comparisons of the experimental waste PE mass fraction and the pyrolysis rate, and the predicted ones by the adaptive neural fuzzy model from 5 °C/min (a), 10 °C/min (b), 15 °C/min (c) to 20 °C/min (d).

respectively. The R-squared values were very close to 1, which revealed high accuracy of the adaptive neural fuzzy model predicted mass fraction. In reference [44], the genetic algorithm was adopted to conduct the kinetic modeling waste PE. The average R-squared value of mass fraction was 0.9992, which is lower than this study's result. Ibrahim and Al-Yaari [17] utilized Arrhenius and Coats-Redfern methods and the artificial neural network model to conduct the recycled low-density PE kinetic modeling. The average mass fraction R-squared values by Arrhenius and Coats-Redfern methods were merely 0.9724 and 0.9401, respectively. While the average R-squared value of mass fraction between artificial neural network model predicted and experimental data was larger than 0.9999. It indicates that machine learning methods are suitable for conducting plastic pyrolysis kinetic modeling.

Regarding the pyrolysis rate, the predicted values were more accurate at the heating rates of 5 and 20 °C/min, as demonstrated in Figure 10a, d. Moreover, as shown in Figure 11b, the R-squared values between the experimental and the predicted pyrolysis rates were 0.99972, 0.99969, 0.99945, and 0.99991 at 5, 10, 15 and 20 °C/min, respectively. The average R-squared value of the genetic algorithm's waste PE pyrolysis rate was merely 0.9772 in the literature [44]. In conclusion, the adaptive neural fuzzy model was accurate in both the mass fraction calculations, R-squared values were close to 1, and the pyrolysis rate calculations, R-squared values were larger than 0.999.

3.4. SA parameters determination

This study utilized the SA to calculate optimal virgin's operating parameters and the waste PE conversions and pyrolysis rates in different
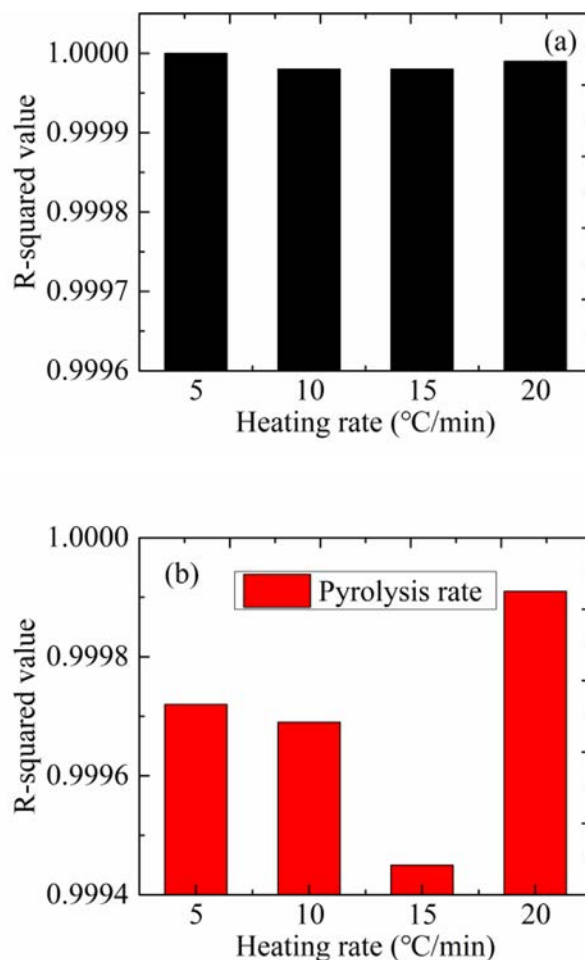

Figure 11. R-squared values of the experimental and the predicted waste PE mass fractions (a) and pyrolysis rates (b) at different heating rates.

Table 1. SA parameters used in the illustration of SA optimization process.

Number of particles	Initial temperature	Temperature displacement coefficient	Temperature probability coefficient	Temperature decrease rate
40	20	0.4	0.05	0.99

temperature ranges. The specific calculation processes were discussed in Appendix A. The parameters utilized in the following SA optimization calculations are listed in Table 1.

Figure 12 depicts the SA optimization process. The SA is used to calculate the virgin PE optimal pyrolysis rate. In the beginning, as demonstrated in Figure 12a, 40 randomly distributed particles were generated on the pyrolysis rate surface. After 1000 iterations and the temperature decreased from 20 to 0, 40 particles converged to the peak of the pyrolysis rate surface as shown in Figure 12b. Moreover, the SA optimized pyrolysis rate was 50.02 wt%/min at the heating rate of 20 °C/min and the temperature of 481.29 °C.

3.5. SA optimized results

According to the discussions of subsection 3.1, the pyrolysis processes of the virgin and the waste PE mainly underwent in the temperature range of 390–510 °C. Therefore, this study investigated the virgin and the waste PE optimal conversions and pyrolysis rates in four individual temperature ranges: 390–420, 420–450, 450–480 and 480–510 °C.
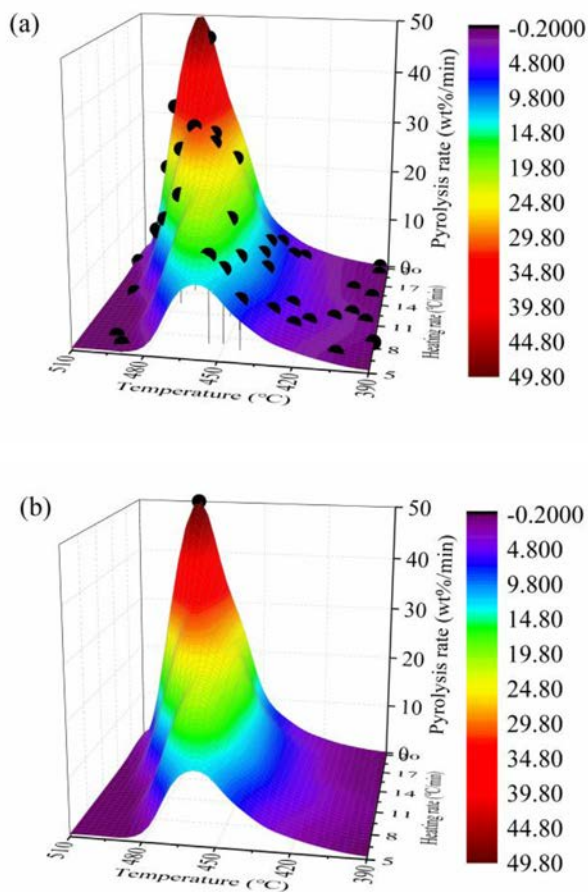

Figure 12. Illustration of SA optimization process with 40 randomly distributed particles (a), to the converged solution (b).

3.5.1. Virgin PE

Figure 13 illustrates the optimal virgin PE conversions in different temperature ranges calculated by the SA. As depicted in Figure 13a, the virgin PE conversion varied from 0.39 to 9.12 % in the temperature range of 390–420 °C. The virgin PE conversion increased with the temperature; it is consistent with the experimental result described in Figure 3. Whereas the conversion increased with the heating rate in the range of about 5–10 °C/min; then the conversion decreased with the heating rate in the range of about 10–20 °C/min. Consequently, the virgin PE optimal conversion was 9.12 % at the temperature of 420 °C, and the heating rate of 9.58 °C/min in the temperature range of 390–420 °C. According to the literature [44], due to different raw materials and varying manufacturing processes, PE's performance differs significantly from materials used in other literature. However, the optimal conversion and pyrolysis rate of this study could still provide references for other polymers. Subsequently, as shown in Figure 13b–d, the virgin PE optimal conversions were 41.75 % at the temperature of 450 °C and the heating rate of 5.02 °C/min in the temperature range of 420–450 °C; 99.53 % at the temperature of 480 °C and the heating rate of 5 °C/min in the temperature range of 450–480 °C; 100.09 % at the temperature of 490.11 °C and the heating rate of 9.03 °C/min in the temperature range of 480–510 °C. It is noteworthy that the optimal virgin PE conversion is larger than 100 % in the temperature range of 480–510 °C. This is because there are still errors between the adaptive neural fuzzy model predicted results and the experimental results. In reference [17], the artificial neural network model predicted conversion also appeared to be greater than 100 %. As demonstrated in Figure 3, the virgin PE mass fraction values were negative in the temperature range of 505.32–510 °C at 10 °C/min. It might be caused by the instrumental error of the thermogravimetric analyzer. Nevertheless, the virgin PE optimal conversions were obtained at higher temperatures. Besides, in the medium temperature ranges, i.e., 420–450 and 450–480 °C, the optimal conversions were obtained at around 5 °C/min heating rate; while in the lower and higher temperature ranges, i.e., 390–420 and 480–510 °C, the optimal conversions were obtained in the heating rate of 9–10 °C/min.

Figure 14 shows the optimal virgin PE pyrolysis rates in different temperature ranges calculated by the SA. As described in Figure 14a,b, the virgin PE pyrolysis rates had a similar variation tendency, which increased with the heating rate in the range of about 5–10 °C/min and decreased with the heating rate in the range of about 10–20 °C/min. Moreover, the pyrolysis rates increased with the temperature in the temperature ranges of 390–420 and 420–450 °C. Furthermore, the SA optimized pyrolysis rates were 4.30 wt%/min at 420 °C and 10.45 °C/min, 17.38 wt%/min at 450 °C and 14 °C/min, 49.77 wt%/min at 480 °C and 20 °C/min, and 50.02 wt%/min at 481.29 °C and 20 °C/min in the temperature ranges of 390–420, 420–450, 450–480 and 480–510 °C, respectively. It could be concluded that a higher optimal pyrolysis rate would be obtained in the higher temperature range. The optimal pyrolysis rates were obtained at higher temperatures in the temperature ranges of 390–420, 420–450 and 450–480 °C. Ulteriorly, in the higher temperature ranges, i.e., 450–480 and 480–510 °C, the optimal pyrolysis rates were obtained at the heating rate of 20 °C/min.

3.5.2. Waste PE

Figure 15 depicts the optimal waste PE conversions in different temperature ranges calculated by the SA. The waste PE conversion has more complex variation trends compared to the virgin PE in Figure 13. Nevertheless, the waste PE conversion increased with the temperature in all temperature ranges. Subsequently, the SA optimized waste PE conversions were 8.48 % at 420 °C and 5 °C/min, 38.71 % at 450 °C and 5
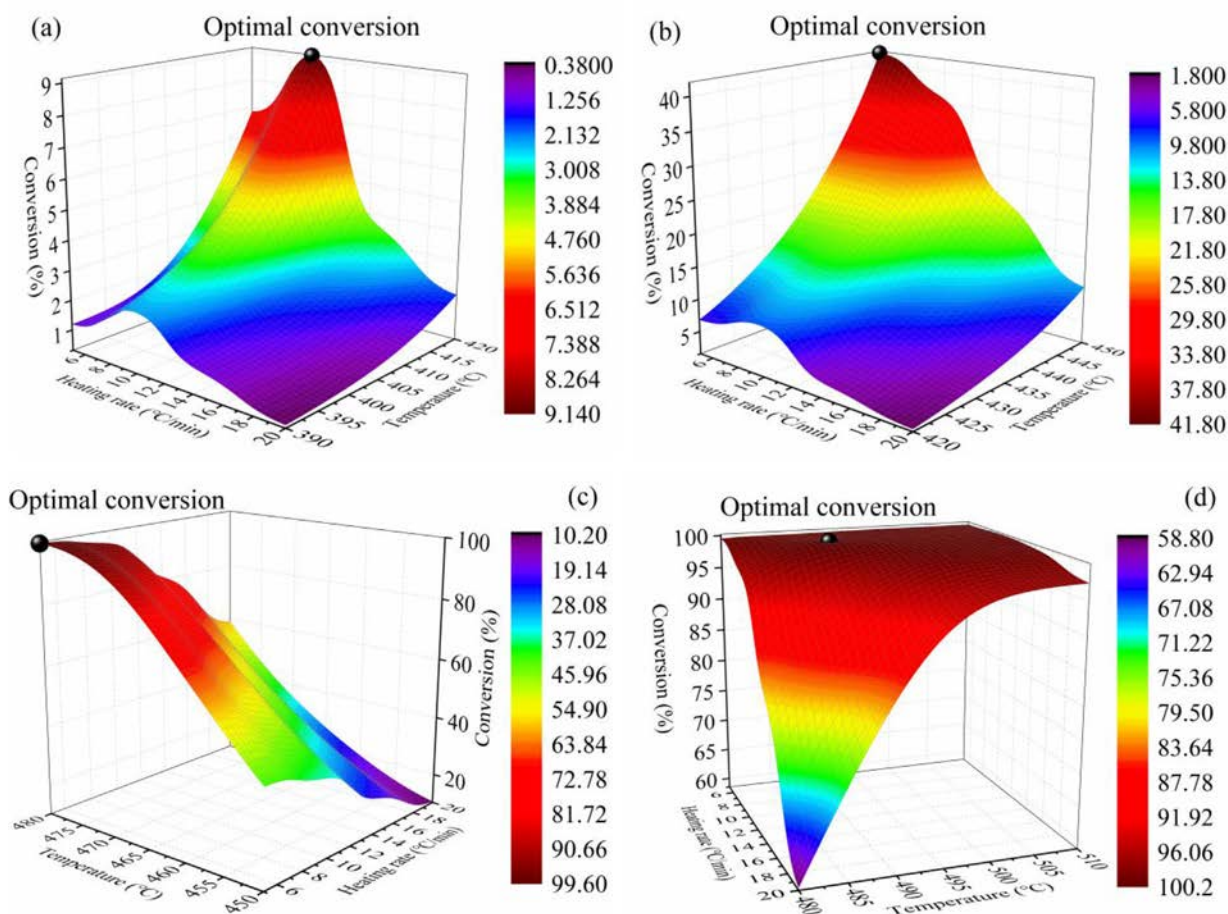
Figure 13. Optimal virgin PE conversions in different temperature ranges calculated by the SA: 390–420 °C (a), 420–450 °C (b), 450–480 °C (c) and 480–510 °C (d).

°C/min, 97.91 % at 480 °C and 5 °C/min, and 99.16 % at 510 °C and 9.82 °C/min in 390–420 °C, 420–450 °C, 450–480 °C, and 480–510 °C ranges, respectively. The optimal heating rate of the waste PE pyrolysis was 5 °C/min in the temperature ranges of 390–420, 420–450 and 450–480. Besides, the waste PE conversion was 98.75 % at 510 °C and 5 °C/min in the temperature range of 480–510 °C. Therefore, it could be concluded that higher temperatures and lower heating rates can enhance waste PE conversion.

Figure 16 demonstrates the optimal waste PE pyrolysis rates in different temperature ranges calculated by the SA. As depicted in Figures 16a, b, the waste PE pyrolysis rates had a similar variation tendency, which increased with the heating rate in the range of about 5–15 °C/min and decreased with the heating rate in the range of about 15–20 °C/min. The waste PE pyrolysis rate increased with the temperature in the temperature ranges of 390–420 and 420–450 °C. Furthermore, the waste PE pyrolysis rates optimized by the SA were 2.91 wt%/min at 420 °C and 14.81 °C/min, 12.91 wt%/min at 450 °C and 14.77 °C/min, 50.18 wt%/min at 480 °C and 20 °C/min, and 52.13 wt%/min at 483.64 °C and 20 °C/min in the temperature ranges of 390–420, 420–450, 450–480 and 480–510 °C, respectively. In conclusion, a higher optimal waste PE pyrolysis rate would be obtained in the higher temperature range. Besides, as the virgin PE in Figure 14, the optimal pyrolysis rates were obtained at higher temperatures in the temperature ranges of 390–420, 420–450, and 450–480 °C. Moreover, within lower temperature ranges, i.e., 390–420 and 420–450 °C, the optimal pyrolysis rates were obtained at the heating rate of about 14.80 °C/min. However, in the higher temperature ranges, i.e., 450–480, and 480–510 °C, the optimal pyrolysis rates were obtained at the heating rate of 20 °C/min.

The adaptive neural fuzzy model, coupled with SA, could be used in other polymers pyrolysis processes. Moreover, it may be utilized to analyze more complex pyrolysis or combustion processes.

4. Conclusion

This study adopted the adaptive neural fuzzy model coupled with SA to investigate the virgin and the waste PE thermal pyrolysis processes for determining the optimal conversions and pyrolysis rates. It is worth mentioning that the optimization method used in this study may be replaced by other computational intelligence algorithms, such as monarch butterfly optimization (MBO), earthworm optimization algorithm (EWA), elephant herding optimization (EHO), moth search (MS) algorithm, etc. The TG experiments at different heating rates were conducted to obtain the experimental data. According to the TG results, the virgin and waste PE's pyrolysis processes took place in the temperature range of 390–510 °C. The waste PE was more challenging to start thermal decomposing compared to the virgin PE. Furthermore, the adaptive neural fuzzy model was adopted to establish the mathematical expressions between the operating parameters, i.e., the pairs temperature and the heating rate, and conversions and pyrolysis rates of the virgin and the waste PE. The R-squared values of the virgin PE conversions (close to 1) and pyrolysis rates (larger than 0.999), and the waste PE conversions (close to 1) and pyrolysis rates (larger than 0.999) revealed the high accuracy of the adaptive neural fuzzy model predicted results. Moreover, SA was utilized to optimize the operating parameters in different temperature ranges; consequently, the SA superior parameters for the optimization calculations were determined. Then, the virgin and the waste PE's optimal conversions and pyrolysis rates were determined by the SA.
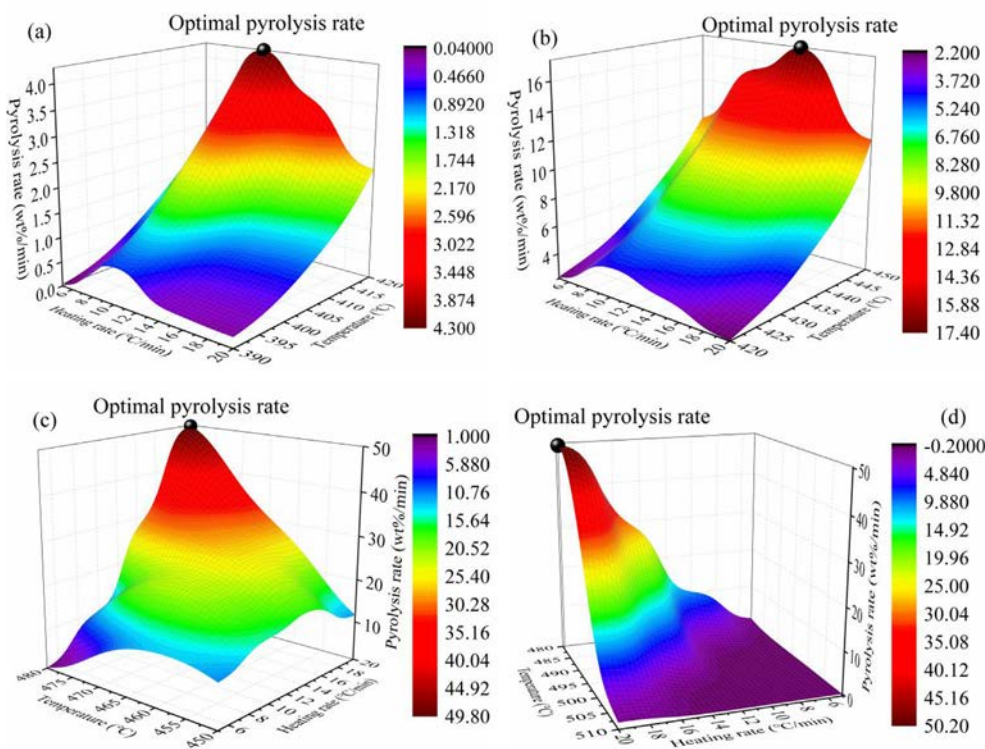
Figure 14. Optimal virgin PE pyrolysis rates in different temperature ranges calculated by the SA: 390–420 °C (a), 420–450 °C (b), 450–480 °C (c) and 480–510 °C (d).
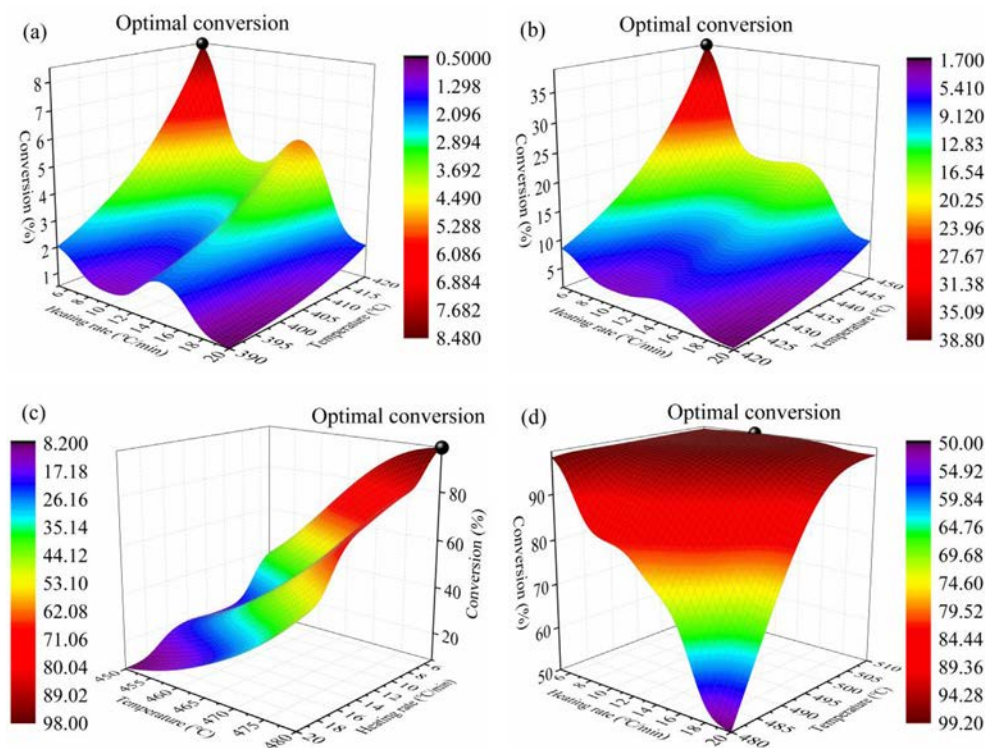

Figure 15. Optimal waste PE conversions in different temperature ranges calculated by the SA: 390–420 °C (a), 420–450 °C (b), 450–480 °C (c) and 480–510 °C (d).

According to the SA optimized results, the optimal conversions of virgin PE were obtained at around 5 °C/min in the medium temperature ranges, i.e., 420–450 °C and 450–480 °C. Whereas the optimal conversions were obtained in the heating rate of 9–10 °C/min in the lower and higher temperature ranges, i.e., 390–420 °C and 480–510 °C. As for the waste PE, the optimal conversions were obtained at 5 °C/min in different temperature ranges. Regarding to the pyrolysis rate, the virgin PE pyrolysis rates optimized by the SA were 4.30 wt%/min at 420 °C and 10.45
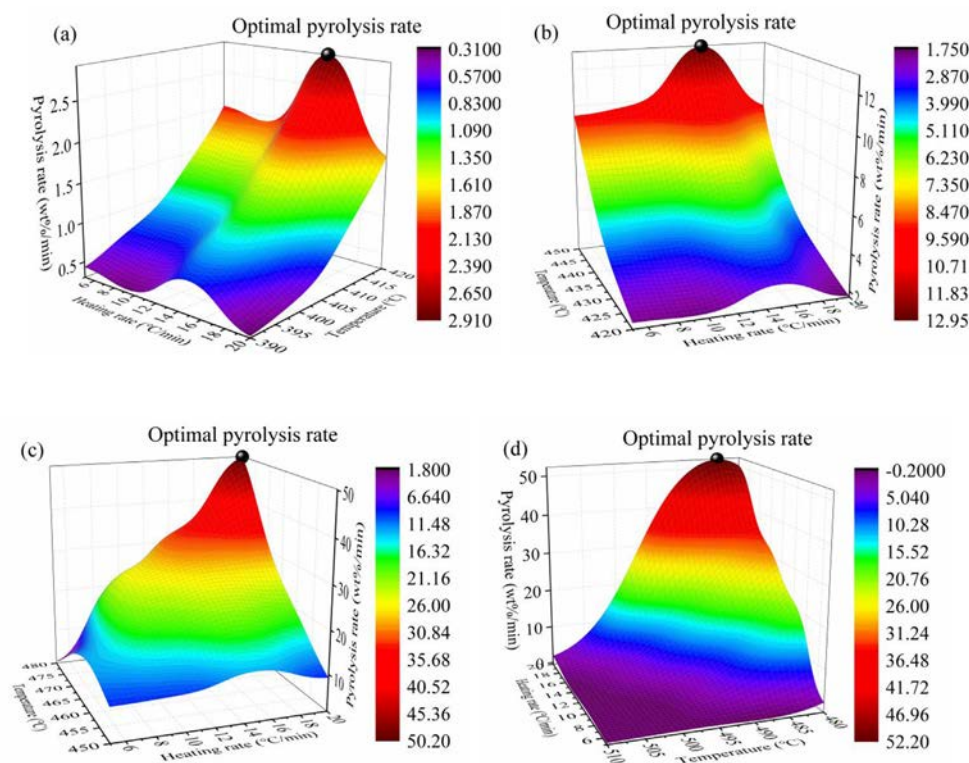
Figure 16. Optimal waste PE pyrolysis rates in different temperature ranges calculated by the SA: 390–420 °C (a), 420–450 °C (b), 450–480 °C (c) and 480–510 °C (d).

°C/min, 17.38 wt%/min at 450 °C and 14 °C/min, 49.77 wt%/min at 480 °C and 20 °C/min, and 50.02 wt%/min at 481.29 °C and 20 °C/min in the temperature ranges of 390–420, 420–450, 450–480 and 480–510 °C, respectively. Moreover, the SA optimized pyrolysis rates of the waste PE were 2.91 wt%/min at 420 °C and 14.81 °C/min, 12.91 wt%/min at 450 °C and 14.77 °C/min, 50.18 wt%/min at 480 °C and 20 °C/min, and 52.13 wt%/min at 483.64 °C and 20 °C/min in the temperature ranges of 390–420 °C, 420–450 °C, 450–480 °C, and 480–510 °C, respectively.

Declarations

Author contribution statement

Ruming Pan: Analyzed and interpreted the data; Contributed reagents, materials, analysis tools or data; Wrote the paper.

João Vitor Ferreira Duque: Conceived and designed the experiments; Performed the experiments; Contributed reagents, materials, analysis tools or data; Wrote the paper.

Márcio Ferreira Martins & Gérald Debenest: Analyzed and interpreted the data; Wrote the paper.

Funding statement

This work was supported by the China Scholarship Council (CSC) program.

Data availability statement

Data will be made available on request.

Declaration of interests statement

The authors declare no conflict of interest.

Additional information

Supplementary content related to this article has been published online at https://doi.org/10.1016/j.heliyon.2020.e05598.

References

[1] T.P. Paula, M.F.V. Marques, M.R.D. Marques, Influence of mesoporous structure ZSM-5 zeolite on the degradation of Urban plastics waste, J. Therm. Anal. Calorim. 138 (5) (2019) 3689–3699.

[2] E. Santos, B. Rijo, F. Lemos, M.A.N.D.A. Lemos, A catalytic reactive distillation approach to high density polyethylene pyrolysis - Part 1 - Light olefin production, Chem. Eng. J. 378 (2019) 122077.

[3] L. Canopoli, F. Coulon, S.T. Wagland, Degradation of excavated polyethylene and polypropylene waste from landfill, Sci. Total Environ. 698 (2020) 134125.

[4] W. Mateo, H.W. Lei, E. Villota, M. Qian, Y.F. Zhao, E.G. Huo, Q.F. Zhang, X.N. Lin, C.X. Wang, Z.Y. Huang, Synthesis and characterization of sulfonated activated carbon as a catalyst for bio-jet fuel production from biomass and waste plastics, Bioresour. Technol. 297 (2020) 122411.

[5] PlasticsEurope, Plastics - the Facts 2017: an Analysis of European Plastics Production, Demand and Waste Data, 2017. https://www.plasticseurope.org/applic ation/files/1715/2111/1527/Plastics_the_facts_2017_FINAL_for_website.pdf.

[6] Z. Dobo, Z. Jakab, G. Nagy, T. Koos, K. Szemmelveisz, G. Muranszky, Transportation fuel from plastic wastes: production, purification and SI engine tests, Energy 189 (2019) 116353.

[7] Y.K. Park, B. Lee, H.W. Lee, A. Watanabe, J. Jae, Y.F. Tsang, Y.M. Kim, Co-feeding effect of waste plastic films on the catalytic pyrolysis of Quercus variabilis over microporous HZSM-5 and HY catalysts, Chem. Eng. J. 378 (2019) 122151.

[8] M. Utami, W. Trisunaryanti, K. Shida, M. Tsushida, H. Kawakita, K. Ohto, K. Wijaya, M. Tominaga, Hydrothermal preparation of a platinum-loaded sulphated nanozirconia catalyst for the effective conversion of waste low density polyethylene into gasoline-range hydrocarbons, RSC Adv. 9 (71) (2019) 41392–41401.

[9] S. Tomasek, Z. Varga, J. Hancsok, Production of jet fuel from cracked fractions of waste polypropylene and polyethylene, Fuel Process. Technol. 197 (2020) 106197.

[10] V.L. Mangesh, S. Padmanabhan, P. Tamizhdurai, A. Ramesh, Experimental investigation to identify the type of waste plastic pyrolysis oil suitable for conversion to diesel engine fuel, J. Clean. Prod. 246 (2020) 119066.

[11] I. Barbarias, G. Lopez, J. Alvarez, M. Artetxe, A. Arregi, J. Bilbao, M. Olazar, A sequential process for hydrogen production based on continuous HDPE fast pyrolysis and in-line steam reforming, Chem. Eng. J. 296 (2016) 191–198.

[12] R.A.M. Esfahani, L. Osmieri, S. Specchia, S. Yusup, A. Tavasoli, A. Zamaniyan, H-2-rich syngas production through mixed residual biomass and HDPE waste via

integrated catalytic gasification and tar cracking plus bio-char upgrading, Chem. Eng. J. 308 (2017) 578–587.

[13] E. Rodriguez, A. Gutierrez, R. Palos, F.J. Vela, M.J. Azkoiti, J.M. Arandes, J. Bilbao, Co-cracking of high-density polyethylene (HDPE) and vacuum gasoil (VGO) under refinery conditions, Chem. Eng. J. 382 (2020) 122602.

[14] S.M. Al-Salem, A. Antelava, A. Constantinou, G. Manos, A. Dutta, A review on thermal and catalytic pyrolysis of plastic solid waste (PSW), J. Environ. Manag. 197 (2017) 177–198.

[15] S.D.A. Sharuddin, F. Abnisa, W.M.A.W. Daud, M.K. Aroua, A review on pyrolysis of plastic wastes, Energy Convers. Manag. 115 (2016) 308–326.

[16] S.Y. Teng, A.C.M. Loy, W.D. Leong, B.S. How, B.L.F. Chin, V. Masa, Catalytic thermal degradation of Chlorella vulgaris: evolving deep neural networks for optimization, Bioresour. Technol. 292 (2019) 121971.

[17] I. Dubdub, M. Al-Yaari, Pyrolysis of low density polyethylene: kinetic study using TGA data and ANN prediction, Polym. Bull. 12 (4) (2020) 891.

[18] S.V. Ustun, M. Demirtas, Modeling and control of V/f controlled induction motor using genetic-ANFIS algorithm, Energy Convers. Manag. 50 (3) (2009) 786–791.

[19] E. Betiku, V.O. Odude, N.B. Ishola, A. Bamimore, A.S. Osunleke, A.A. Okeleye, Predictive capability evaluation of RSM, ANFIS and ANN: a case of reduction of high free fatty acid of palm kernel oil via esterification process, Energy Convers. Manag. 124 (2016) 219–230.

[20] B.O. Ighose, I.A. Adeleke, M. Damos, H.A. Junaid, K.E. Okpalaeke, E. Betiku, Optimization of biodiesel production from Thevetia peruviana seed oil by adaptive neuro-fuzzy inference system coupled with genetic algorithm and response surface methodology, Energy Convers. Manag. 132 (2017) 231–240.

[21] A. Khosravi, S. Syri, J.J.G. Pabon, O.R. Sandoval, B.C. Caetano, M.H. Barrientos, Energy modeling of a solar dish/Stirling by artificial intelligence approach, Energy Convers. Manag. 199 (2019) 112021.

[22] M. Aghbashlo, M. Tabatabaei, S. Hosseinpour, H. Rastegari, H.S. Ghaziaskar, Multi-objective exergy-based optimization of continuous glycerol ketalization to synthesize solketal as a biodiesel additive in subcritical acetone, Energy Convers. Manag. 160 (2018) 251–261.

[23] H. Sayyaadi, M. Babaie, M.R. Farmani, Implementing of the multi-objective particle swarm optimizer and fuzzy decision-maker in exergetic, exergoeconomic and environmental optimization of a benchmark cogeneration system, Energy 36 (8) (2011) 4777–4789.

[24] H. Sayyaadi, M. Baghsheikhi, Developing a novel methodology based on the adaptive neuro-fuzzy interference system for the exergoeconomic optimization of energy systems, Energy 164 (2018) 218–235.

[25] H. Sayyaadi, M. Baghsheikhi, Retrofit of a steam power plant using the adaptive neuro-fuzzy inference system in response to the load variation, Energy 175 (2019) 1164–1173.

[26] S. Kirkpatrick, C.D. Gelatt, M.P. Vecchi, Optimization by simulated annealing, Science 220 (4598) (1983) 671–680.

[27] M. Paraschiv, R. Kuncser, M. Tazerout, T. Prisecaru, New energy value chain through pyrolysis of hospital plastic waste, Appl. Therm. Eng. 87 (2015) 424–433.

[28] Y. Jamal, M. Kim, H.S. Park, Isothermal combustion kinetics of synthetic refuse plastic fuel (RPF) blends by thermogravimetric analysis, Appl. Therm. Eng. 104 (2016) 16–23.

[29] L. Chen, S.Z. Wang, H.Y. Meng, Z.Q. Wu, J. Zhao, Synergistic effect on thermal behavior and char morphology analysis during co-pyrolysis of paulownia wood blended with different plastics waste, Appl. Therm. Eng. 111 (2017) 834–846.

[30] R.Y. Chen, X.K. Xu, Y. Zhang, S.M. Lo, S.X. Lu, Kinetic study on pyrolysis of waste phenolic fibre-reinforced plastic, Appl. Therm. Eng. 136 (2018) 484–491.

[31] L.C. Ge, H.C. Feng, C. Xu, Y.W. Zhang, Z.H. Wang, Effect of hydrothermal dewatering on the pyrolysis characteristics of Chinese low-rank coals, Appl. Therm. Eng. 141 (2018) 70–78.

[32] K. Aghajani, H.A. Tayebi, Adaptive Neuro-Fuzzy Inference system analysis on adsorption studies of Reactive Red 198 from aqueous solution by SBA-15/CTAB composite, Spectrochim. Acta A Mol. Biomol. Spectrosc. 171 (2017) 439–448.

[33] S.M. Mousavi, E.S. Mostafavi, P.C. Jiao, Next generation prediction model for daily solar radiation on horizontal surface using a hybrid neural network and simulated annealing method, Energy Convers. Manag. 153 (2017) 671–682.

[34] Y. Luo, T. Lu, X.Z. Du, Novel optimization design strategy for solar power tower plants, Energy Convers. Manag. 177 (2018) 682–692.

[35] W.P. Zhang, A. Maleki, M.A. Rosen, J.Q. Liu, Sizing a stand-alone solar-wind-hydrogen energy system using weather forecasting and a hybrid search optimization algorithm, Energy Convers. Manag. 180 (2019) 609–621.

[36] M. Tahani, N. Babayan, A. Pouyaei, Optimization of PV/Wind/Battery stand-alone system, using hybrid FPA/SA algorithm and CFD simulation, case study: Tehran, Energy Convers. Manag. 106 (2015) 644–659.

[37] K.G. Xie, J.Z. Dong, H.M. Tai, B. Hu, H.L. He, Optimal planning of HVDC-based bundled wind–thermal generation and transmission system, Energy Convers. Manag. 115 (2016) 71–79.

[38] P. Das, P. Tiwari, Thermal degradation kinetics of plastics and model selection, Thermochim. Acta 654 (2017) 191–202.

[39] Z. Wang, R.C. Wei, X.Y. Ning, T. Xie, J. Wang, Thermal degradation properties of LDPE insulation for new and aged fine wires, J. Therm. Anal. Calorim. 137 (2) (2019) 461–471.

[40] J.V.F. Duque, M.F. Martins, G. Debenest, M.T.D. Orlando, The influence of the recycling stress history on LDPE waste pyrolysis, Polym. Test. 86 (2020) 106460.

[41] P. Das, P. Tiwari, Thermal degradation study of waste polyethylene terephthalate (PET) under inert and oxidative environments, Thermochim. Acta 679 (2019) 178340.

[42] A. Aboulkas, K. El Harfi, A. El Bouadili, Thermal degradation behaviors of polyethylene and polypropylene. Part I: pyrolysis kinetics and mechanisms, Energy Convers. Manag. 51 (7) (2010) 1363–1369.

[43] S. Kim, Y.C. Kim, Using isothermal kinetic results to estimate the kinetic triplet of the pyrolysis of high density polyethylene, J. Anal. Appl. Pyrolysis 73 (1) (2005) 117–121.

[44] R. Pan, J.V.F. Duque, G. Debenest, Investigating waste plastic pyrolysis kinetic parameters by genetic algorithm coupled with thermogravimetric analysis, Waste Biomass Valori (2020).